

LIQUEFACTION OPPORTUNITY MAPPING VIA SEISMIC WAVE ENERGY

By M. I. Todorovska¹ and M. D. Trifunac²

ABSTRACT: An empirical, energy-based methodology for liquefaction hazard assessment and microzonation mapping is presented. The approach is probabilistic, considers the uncertainty in the liquefaction criterion, and is applicable to most earthquake-induced liquefaction analyses. The examples illustrated are for water-saturated sands at level ground. The energy of ground shaking is estimated from the Fourier amplitude spectra of the incident waves. The susceptible materials are characterized only by their corrected standard penetration test value \bar{N} and overburden pressure σ_0 . Illustrative microzonation maps of liquefaction opportunity are shown for the Los Angeles metropolitan area. Two types of maps are presented, one showing the average return period of liquefaction occurrence (for given \bar{N} and σ_0), and another one showing distribution of \bar{N} with equal probability to liquefy during 50 years exposure (for given σ_0). An advantage of the method is that the result is given directly in terms of in situ albeit simple soil characteristics rather than in terms of laboratory tests and peak acceleration. Possible applications of the computed opportunity maps are discussed.

INTRODUCTION

Liquefaction of water-saturated sands is believed to occur when the pore pressure approaches the confining pressure, so that the material changes the state from solid to liquid (Kramer 1996). When a layer liquefies, the ground loses strength, and movement of large blocks of soil can be initiated (lateral spreading), causing damage to man-made structures. The need for mapping a liquefaction hazard was recognized after the 1964 Niigata (Japan) and Alaska (U.S.) earthquakes, and mapping started in the early 1970s. Youd (1991) presents a state-of-the-art review of methodologies and case studies of liquefaction mapping worldwide. The mapping procedures are divided into three groups: (1) Susceptibility mapping (of areas that can liquefy if subjected to sufficiently strong and long ground shaking); (2) opportunity mapping (of areas exposed to earthquake shaking capable of initiating liquefaction); and (3) potential mapping (of areas where there is both opportunity and susceptible material for liquefaction to occur).

This paper illustrates the application of an energy-based methodology to microzonation mapping of liquefaction opportunity on level ground. The methodologies for opportunity mapping applied so far (Youd 1991) are based on: (1) magnitude-distance relation (Yegian and Whitman 1978; Youd and Perkins 1978; Tinsley et al. 1985); (2) magnitude-maximum acceleration relations (Atkinson et al. 1984; Kavazanjian et al. 1985); and (3) liquefaction severity index (Youd and Perkins 1987). The first two types consider only the initiation of liquefaction, whereas the third also considers the consequences. The magnitude-distance relations' methodologies are based on the simplest two-parameter characterization of strong shaking and decay of ground motion amplitudes with distance due to attenuation along the wave path. The magnitude-maximum acceleration relations' methodologies consider ground accelerations at the site and use magnitude as a measure of the duration of shaking.

Peak acceleration has been the most widely mapped characteristic of strong ground shaking (Algermissen and Perkins 1976) and has been used in many applications. Unfortunately, it is a poor indicator of the energy of ground motion and of

the potential for damage. Response spectral amplitudes have also been mapped as an indicator of the level of structural response during ground shaking (Lee and Trifunac 1987; Lee 1993). However, no soil liquefaction criterion, at least of those widely used, is based on spectral characterization of ground motion. Spectral intensity (Benioff 1934) and the Arias intensity [proportional to $\int a^2(t) dt$, where $a(t)$ is absolute ground acceleration and t is time (Trifunac and Brady 1975)] are sometimes used as measures of the destructive effects of ground shaking on structures, and recently for the assessment of liquefaction potential (Kayen and Mitchell 1997). These intensities can be related to the energy dissipated by single degree-of-freedom oscillators with frequencies in an interval (ω_L, ω_R) (for the Arias intensity, $\omega_L = 0$ and $\omega_R = \infty$) during the entire duration of the excitation. Liquefaction occurrence, however, should be correlated with the energy of seismic waves propagating through the soil, which is proportional to $\int v^2(t) dt$, where v is ground velocity (Trifunac 1972, 1999). This energy can be evaluated using various functionals, engaging different characteristics of shaking [e.g., broadband Fourier amplitude spectra of acceleration, peak velocity and duration of shaking, and Fourier amplitude spectra of velocity (Trifunac 1995)].

In this paper, the "en" model of Trifunac (1995) is briefly reviewed, and its incorporation within the framework of probabilistic seismic hazard analysis is discussed. Then, illustrations and discussion follow on the application of this methodology to microzonation of the Los Angeles metropolitan area. Application of the models of Trifunac (1995) to probabilistic seismic hazard assessment was first presented by Todorovska (1996), with illustrations for one fault only (modeled by a vertical surface). The purpose of the study was to examine how sensitive the results are on the model used, on the lower cutoff magnitude contributing to the hazard, and on Gaussian versus truncated Gaussian probability distribution function assumed for the model. The aim of this paper is to illustrate an application of the methodology to seismic zoning (spatial distribution of the hazard) for a realistic seismic environment (consisting of many seismic sources), and to explore possible future uses of microzonation maps.

The two main advantages of Trifunac's (1995) "en" model (energy $\sim \int v^2 dt$) over the conventional models are that: (1) It accounts for the effects of the local soil and site geology both on amplitudes and duration of strong shaking; and (2) it uses frequency-dependent attenuation function. The former includes amplitude amplification and prolonged duration of strong motion by deep sediments, resulting in larger energy input available to build up the pore pressure at the site. The latter, in the framework of our hazard model, weighs the contributions from different asperities at the source in a manner analogous to the closest distance to the fault. The amplification

¹Res. Assoc. Prof., Civ. Engrg. Dept., Univ. of Southern California, Los Angeles, CA 90089-2531.

²Prof., Civ. Engrg. Dept., Univ. of Southern California, Los Angeles, CA.

Note. Discussion open until May 1, 2000. To extend the closing date one month, a written request must be filed with the ASCE Manager of Journals. The manuscript for this paper was submitted for review and possible publication on May 2, 1996. This paper is part of the *Journal of Geotechnical and Geoenvironmental Engineering*, Vol. 125, No. 12, December, 1999. ©ASCE, ISSN 1090-0241/99/0012-1032-1042/\$8.00 + \$.50 per page. Paper No. 13173.

of strong motion by sediments is more significant for longer periods [e.g., >0.2–0.5 s for strong motion velocity (Trifunac 1976a, 1993)]. An advantage of the “en” model over the Arias intensity-based model by Kayen and Mitchell (1997) is that it is based on the direct representation of energy of the wave motion in a continuum ($\sim \int v^2 dt$; recall the discussion in the third paragraph in this section). A drawback of the Arias intensity ($\sim \int a^2 dt$) based model relative to the “en” model is that the ground acceleration that the Arias intensity is based on is a high-frequency characteristic of strong motion, and therefore, is less sensitive to the amplification and prolonged duration of shaking on sediments (more pronounced for intermediate and long periods). Another consideration is that, for large amplitudes of shaking near the earthquake source [$v(t) \geq 20$ cm/s], the Fourier amplitude spectra at high frequencies (periods ≤ 0.2 –0.5 s) and the peak accelerations can be reduced by nonlinear site response (Trifunac and Todorovska 1996, 1998a,c). As a result, $\int a^2 dt$ and to a lesser degree of $\int v^2 dt$, will underestimate the incident wave energy, when computing directly from recorded motions.

The methodology illustrated in this paper uses the simplest possible field characterization of the soil by a corrected standard penetration test (SPT) value. The SPT is a commonly used in situ test. The cone penetration test (CPT) is also becoming a popular in situ test. It is believed to be more reliable, economical, fast, and standardized for the continuous measurement of penetration resistance q_c (Robertson et al. 1992). It is not used more often for the characterization of liquefaction resistance, despite the good body of data for the development of CPT-based correlations, because these require knowledge of the fines content of the soil, which is not obtained from the CPT other than through approximate correlations. The liquefaction occurrence does depend on other site-specific parameters [e.g., grain size distribution, initial relative density, initial effective stress, amplitude of the excitation, and duration of shaking (Blazquez et al. 1980)], and the use of corrected SPT values to represent some of those parameters collectively represents only a rough first-order approximation.

METHODOLOGY

A methodology for probabilistic mapping of a liquefaction hazard requires a model of the sources of possible earthquakes that may cause liquefaction (spatial, magnitude, and temporal distribution), and a description of ground motion at a site from the possible earthquakes that can lead to liquefaction. The following will describe those elements, as used in this paper.

Model of Seismic Sources

The seismicity model used in this paper is a modification of models used earlier by other authors (Lee and Trifunac 1987; Todorovska 1994a, 1995a,b; Todorovska et al. 1995; Todorovska and Trifunac 1996). The source zones are lines (along the traces of the major faults) or regions of “diffused seismicity” [enclosed by dashed lines (Fig. 1)]. They are labeled by a number, and their names, seismic moment rates M_0 , and maximum magnitudes M_{max} are listed in Table 1. The moment rates are consistent with those for the alternate model (Poissonian) proposed by the working group on California earthquake probabilities (WGCEP) (Working 1995). The geometry and segmentation of the source zones and the magnitude distribution of the seismic moment rate are different. The model in this paper is simpler in that it has a smaller number of segments (by combining shorter segments of the major faults, e.g., of the San Andreas and San Jacinto Faults, into fewer longer segments with a moment rate equal to the sum of the rates assigned to the individual segments). This simplification eliminates the need for the cascade model, which allows several shorter contiguous segments of the major faults to rupture together during a single larger magnitude event. In the illustrations in this paper, the earthquakes in the fault zones occur along buried lines at 8.5 km depth [approximately the equivalent depth for a vertical surface fault (Todorovska and Lee 1995)]. An exception is the Simi-San Fernando Zone (No. 33), which is modeled by a surface of diffused seismicity. The other diffused seismicity zone (No. 34) encloses the entire region (southern California), and accounts for earthquakes that

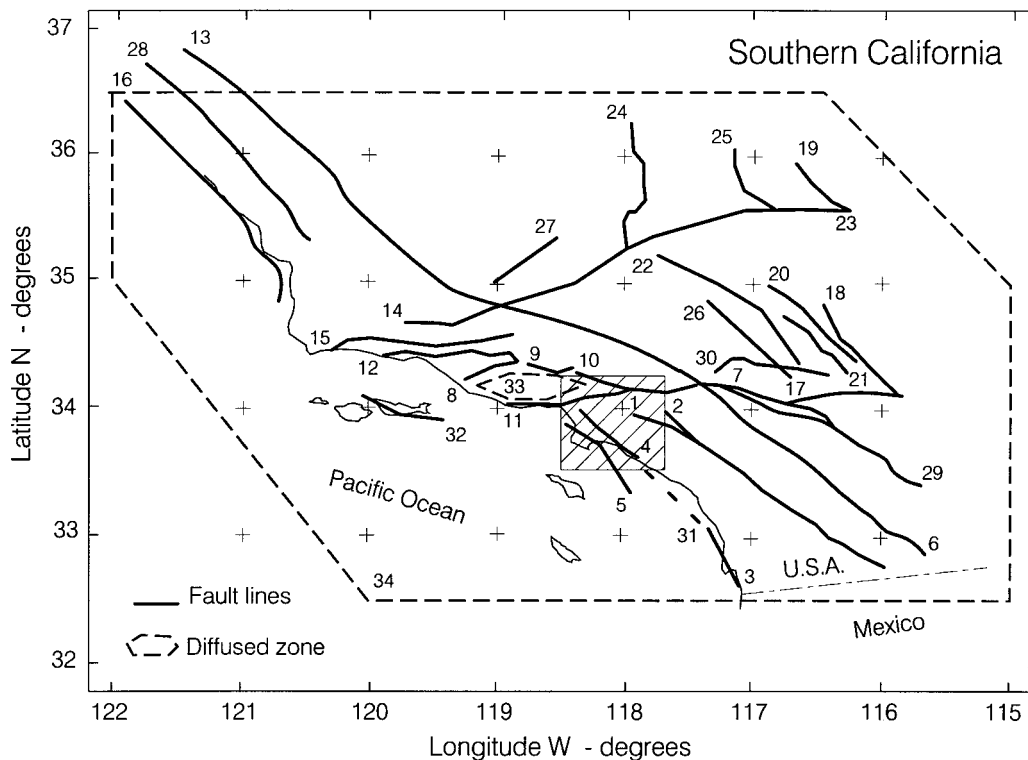


FIG. 1. Major Faults in Southern California, also Listed in Table 1. Dashed Polygons Represent Regions of Diffused Seismicity. Small Hatched Rectangle Is Area Considered for Microzoning in this Paper. [Modified from Lee and Trifunac (1987)]

TABLE 1. Southern California Seismicity Model—Moment Rates^a

Fault name (1)	$M_0^d \times 10^{22}$ (dyn-cm/year) (2)	$M_0^c \times 10^{22}$ (dyn-cm/year) (3)	M_{max} (4)
Elsinore-Whittier Fault	54	317	7.8
Chino Fault	5	15	7.4
Rose Canyon Fault	17	15	7.4
Newport-Inglewood Fault Zone	17	24	7.3
Palos Verde Fault	28	50	7.6
San Jacinto Fault Zone	75	811	7.9
San Andreas, Cajon Pass to Imperial Valley on North Branch	50	780	8.0
Oakridge Fault	44	0	7.6
Santa Susana Fault	22	2	7.5
Sierra Madre-Cucamonga Fault Zone	63	18	7.8
Malibu Coast-Santa Monica-Raymond Fault System	30	24	7.6
Arroyo Parida-San Cayetano Fault Zone	89	0	7.8
San Andreas Fault-Cajon Pass to San Luis Obispo	189	3,497	8.0
Big Pine Fault	13	0	7.4
Santa Ynez Fault	83	0	7.6
San Gregorio-Hosgri Fault Zone	61	25	7.7
Pinto Mountain Fault	18	1	7.3
Pisgan-Bullion Fault	32	0	7.7
South Death Valley Fault	43	0	7.7
Calico-West Calico Fault	32	0	7.7
Camp Rock-Emerson Fault Zone	32	0	7.7
Lockhart-Lenwood Fault	32	0	7.7
Garlock Fault	128	169	8.0
Sierra Nevada Fault	37	0	7.6
Panamint Valley Fault	44	0	7.7
Elendale Fault	32	0	7.8
White Wolf Fault	106	0	7.8
Rinconada Fault	39	0	7.4
San Andreas, Cajon Pass to Imperial Valley on South Branch	50	780	8.0
North Frontal Fault	31	0	7.0
Santa Cruz Fault	19	6	7.5
Newport-Inglewood Fault-Offshore	13	15	7.4
Simi-San Fernando Zone	21	57	7.3
Diffused Seismicity Zone	1,493	0	7.5

^aFor distributed and characteristic earthquakes M_0^d and M_0^c , respectively, and maximum magnitude M_{max} .

may occur away from the line source zones. The model adopted in this paper (Fig. 1 and Table 1) covers approximately the same area and has the same integral moment rate (over all of the source zones) as the alternate model of the WGCEP (Working 1995).

The WGCEP (Working 1995) classified all of the source zones into A, B, and C categories, depending on the detail of information available. For Zones A and B, two populations of earthquakes were assumed, one occurring randomly in time (as a Poissonian sequence), with frequency specified by a linear Gutenberg-Richter relationship, $\log n_{eq} = a - bM$ (Richter 1958), and magnitudes between $M = 6$ and $M = M_{max}$, and another one with “characteristic” earthquakes with $M = M_{max}$. These two populations are assigned seismic moment rates M_0^d and M_0^c . The characteristic earthquakes for Zone B are also Poissonian as well as for Zone A in the alternate model. In the preferred model, a time-dependent hazard model was used for Zone A events, accounting for the elapsed time since the most recent characteristic event on the particular fault segment.

In this paper, the characteristic earthquakes were assumed to be Poissonian for both Zones A and B, with magnitudes between $M = 6.75$ and M_{max} , and frequency of occurrence $\log n_{eq} = a - bM$, with $b = 0.5$. The “random” or “distributed” earthquakes were assumed to be Poissonian in all of the zones, with magnitudes between $M = 2.75$ and M_{max} , and frequency of occurrence $\log n_{eq} = a - bM$, with $b = 1.0$. In the calculations, the magnitude was discretized with a step of 0.5 units, and M refers to the center of the interval. The seismic moment rates and M_{max} are listed in Table 1. Fig. 2 shows the occurrence rate of earthquakes with magnitudes greater than M predicted by the model adopted in this paper (heavy solid line)

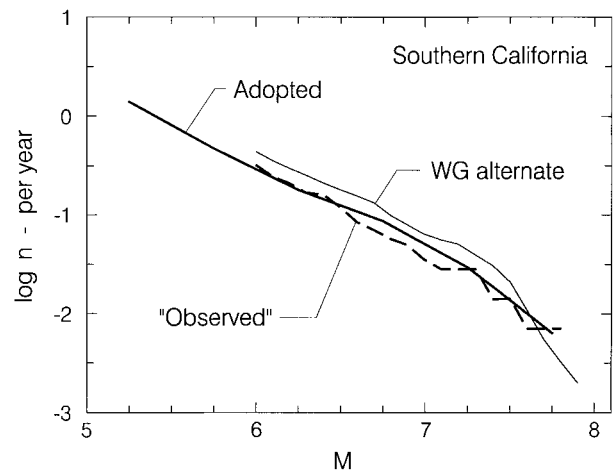


FIG. 2. Gutenberg-Richter Relationship for Model Adopted in this Paper and for Alternate Model of WGCEP (1995), Plotted against Rate Observed since 1850 ($M \geq 6$, Aftershocks Removed)

and by the alternate model of the WGCEP (Working 1995) (thin solid line) for the whole region. The dashed line corresponds to the observed earthquakes [$M > 6$ only, aftershocks excluded (Working 1995)]. It is seen that for $M < 7.625$, the adopted model predicts a smaller number of earthquakes than the WGCEP alternate model, but agrees with the observed long-term rate.

Despite the large uncertainties and ambiguities in modeling seismic sources, the probabilistic seismic hazard analysis is a powerful tool for the assessment of hazards and risks caused by earthquakes, and for developing design standards, because

it considers, in a balanced way, the likelihood of the earthquake occurrences, their effects at the site, and considers simultaneously contributions to the hazard from all known (so far) seismic sources. Also, it allows a relative comparison of earthquake-caused risks (of loss of life, injury, and monetary losses), with risks caused by various other natural or man-made hazards [e.g., environmental, health, and traffic accidents (Fischhoff et al. 1981)], and therefore helps in decision-making processes.

Liquefaction Criterion

The initiation of liquefaction in water-saturated cohesionless sands is assumed to occur when the effective stress in the ground approaches zero. Starting from this hypothesis, Davis and Berrill (1982) formulated energy-based empirical criteria for liquefaction, which were later refined by Berrill and Davis (1985) and Trifunac (1995). The methodology employed in this paper uses the criteria proposed by Trifunac (1995), briefly reviewed in the following.

Energy Methods and “en” Model

Let σ_0 and \bar{N} be the overburden pressure and the corrected (for overburden pressure) SPT value for a liquefiable sand layer, and let E be the seismic wave energy arriving at that site. Part of this energy will be dissipated in the soil and will contribute toward pore pressure buildup. The dissipated energy is assumed to be proportional to $f(\bar{N})\sigma_0^{-1}E$, where f is some function, and the increase in pore pressure Δu is then proportional to (Davis and Berrill 1982)

$$\Delta u \sim \frac{f(\bar{N})}{\sigma_0^{1/2}} E \quad (1)$$

In the absence of other loads, on level ground, the Δu required just to initiate liquefaction should be approximately equal to σ_0 , which leads to

$$f(\bar{N}) \sim \sigma_0^{3/2}/E \quad (2)$$

Different functional forms for E (in terms of the earthquake and site parameters) can lead to different liquefaction initiation criteria, and can be calibrated based on empirical data. One such model is the “en” model of Trifunac (1995), which was used to calculate the results presented in this paper.

The wave energy of strong motion in the soil at a site is proportional to (Trifunac 1972, 1999)

$$E \sim \int_0^{t_0} v^2(t) dt \quad (3)$$

where t_0 = total duration of strong motion shaking; and v = ground velocity at the site. From the Parseval’s theorem (Papoulis 1962), it follows that

$$E \sim \int_0^\infty \left(\frac{F(\omega)}{\omega} \right)^2 d\omega \quad (4)$$

where $F(\omega)$ = amplitude of Fourier spectrum of strong motion acceleration. The spectrum $F(\omega)$ can be estimated from empirical scaling laws of the form

$$\log F(\omega) = \varphi(M, r, H, \omega, V, h, s, s_L, p) \quad (5)$$

where φ designates a particular regression model, which requires as input, e.g., the earthquake magnitude M ; source to station distance r ; source depth H ; frequency ω ; component of motion ($V = 0$ for horizontal, $V = 1$ for vertical motion); local geologic site conditions [via the thickness of sediments h or the parameter s equal to 0 for sediments, 2 for basement rock, and 1 for intermediates sites (Trifunac 1990a)]; local soil site

conditions [$s_L = 0$ for “rock” sites, 1 for “stiff” sites, and 2 for “deep” soil sites (Trifunac 1990a)]; and the desired confidence of the estimate (p is the probability that the estimate will not be exceeded).

The overall duration of strong motion at the site, when measured from $\int a^2 dt$ or $\int v^2 dt$, is the same (Trifunac and Brady 1975), but the time rate of growth of $\int a^2 dt$ is at first faster than for $\int v^2 dt$, during the first part of a strong motion interval, and faster than the measured (Holzer et al. 1989; Youd and Holzer 1994) buildup of pore-water pressure. For site-specific modeling of pore-pressure buildup with time, empirical scaling in terms of $\int v^2 dt$ appears to be the most appropriate, because $v(t)$ is roughly proportional to the components of strain in the soil (Youd and Holzer 1994).

The current engineering methods for liquefaction assessment have been formulated on the basis of cyclic shear stress, which develops in the soil during excitation by incident earthquake waves (Kramer 1996). The shear stress τ in the soil is proportional to shear strain γ ($\tau \sim \mu\gamma$, where μ is the Lamé modulus for shear deformation, and $\gamma \sim \partial u/\partial x$, with u representing displacement, and x an appropriate coordinate); whereas the strain is proportional to the particle velocity $v(t)$ [$\gamma(t) \sim v(t)/c$, where c is the “representative” phase velocity (Trifunac and Lee 1966)]. A differential of work done by the cyclic shear stress during wave motion in the soil is proportional to $\tau \cdot du$. Integrated over the entire volume in question, and over all time, the result is again proportional to $\int v^2 dt$.

The “en” model uses the broadband scaling laws proposed by Trifunac (1993, 1994), defined for frequencies beyond the range in which typical recorded strong ground motion has a signal-to-noise ratio greater than unity. This range depends on the earthquake magnitude and distance from the source, and is typically 0.1–25 Hz (Lee et al. 1982). Within the recordable range, the spectrum is given by empirical scaling models defined by regression analyses of strong motion data. All of the models use a frequency-dependent attenuation function for strong ground motion and representative source to station distance (Trifunac and Lee 1990), and they differ in the set of parameters describing the effects of the local site conditions (e.g., some models use simultaneously the geologic site characterization and the local soil characterization, whereas others use only the geologic site characterization; the models also differ in whether the geologic site classification is in terms of the categorical variable s or in terms of thickness of sediments h). Outside the recordable frequency band, the spectrum is defined based on the behavior of theoretical Fourier spectrum, and it is calibrated by data on the average fault slip and high-frequency attenuation characteristics of the medium, measured independently. When the integral on the right-hand side of (4) is evaluated for frequencies between 0.01 and 100 Hz, its value, in units m^2/s , will be denoted by “en.”

The liquefaction initiation criterion specified by (2) requires that the function $f(\bar{N})$ is specified. Trifunac (1995) assumed $f(\bar{N}) \sim \bar{N}^{-n}$, where the exponent n and the proportionality factor are determined by regression. The regression analysis for the “en” model gives

$$\bar{N}_{\text{mod}} = c \left[\frac{en}{\sigma_0^{3/2}} \right]^{1/n} \quad (6)$$

with $c = 572$ and $n = 2.5$, for en in m^2/s , σ_0 in kPa, and \bar{N} in counts per foot (1 ft = 30.48 cm). The data set consists of 91 observations worldwide of occurrence as well as nonoccurrence of liquefaction after an earthquake (Davis and Berrill 1982), evidenced by surface manifestations (sand boils, ground fissures, etc.). The constants c and n in (5) are such that the occurrences are separated from the nonoccurrences, in a least-squares sense. The other empirical scaling models proposed by Trifunac (1995) were defined in a similar fashion, but for

different approximate representations of the integral “en,” e.g., directly in terms of magnitude and distance, or in terms of peak velocity (Trifunac 1976b) and duration of strong shaking (Novikova and Trifunac 1993, 1995).

Local Site and Soil Conditions

The characteristics of strong earthquake shaking at a site, and consequently the seismic wave energy and liquefaction opportunity, depend, in a complex and nonlinear way, simultaneously on: (1) the earthquake source (orientation and distribution of slip along the rupture surface); (2) the propagation path (e.g., waveguides, crossing of boundaries of high-impedance contrast, etc.); (3) the regional geology (topography as well as deep geologic structure); and (4) the near-surface geology and local soil. The degree to which each of these factors affects the ground motion at a site is difficult to estimate. The associated effects cannot be easily separated, because of insufficient or inadequate strong motion data for a particular earthquake, and limitations in our knowledge of the geology at depth along the wave path. Linear transfer-function representations of various source, transmission, and site effects are not valid in the near-field region of destructive earthquakes, not only because of the irregular spatial distribution of linear and nonlinear soil response (Trifunac and Todorovska 1996, 1998a,b,c), but also because different bursts of strong motion energy arrive from different asperities on large faults, and therefore arrive along different propagation paths, to be further modified by local focusing, scattering, and diffraction for different incident angles. Because strong earthquake shaking is rare, and the number of recorded accelerograms per earthquake event continues to be small [e.g., only about 200 for the 1994 Northridge, Calif., earthquake (Todorovska and Trifunac 1997a,b)], these complexities are not likely to be resolved in the near future. In the meantime, simplified models will be used in engineering applications, based on our current limited understanding of the mechanism of a few of the associated effects.

Near-surface soils and sedimentary deposits can amplify the amplitudes of motion, as a result of 3D interference and focusing. For large excitations, soft near-surface soils may respond nonlinearly, reducing the acceleration amplitudes, and leading to large strains and permanent deformation. Presently, the site effects on strong motion amplitudes are considered either via some site classification and direct scaling using regression models or by detailed site response studies using rock motion as input. Sites may be classified based only on the shear-wave velocity in the upper 30–40 m below the surface (A, B, C, and D soil classification), based also on the soil depth (e.g., the rock soil, stiff soil, deep soil, and deep cohesionless soil classification), or considering simultaneously the local soil and the deeper geologic structure, through the thickness of sediments or geologic site classification $s = 0$ (sediments), $s = 2$ (rock), and $s = 1$ (intermediate) (Trifunac 1990a). The path effects on the attenuation of strong motion amplitudes were considered for the first time only recently (Lee et al. 1995; Lee and Trifunac 1995a,b), in a simplified manner by classification of path types. Although the focusing and amplification effects will also depend on the horizontal dimensions of the soil and sedimentary deposits, those are usually ignored both in direct scaling models and in site response analyses (Trifunac and Novikova 1995). Site response analyses can model in detail the soil properties, but they usually only consider the interference of vertically propagating shear waves.

Ideally, the analysis of liquefaction should consider at least the previously mentioned site characteristics used in scaling the strong ground motion, as well as other relevant site specific variables (e.g., elevation of the water table). Such supporting data were not available in a systematic and uniform way for

the liquefaction occurrence data, reviewed by Davis and Berill (1982). Therefore, the models of Trifunac (1995) were developed assuming representative site conditions (stiff soil and sediments site geology). For microzonation mapping, it is valuable to show the variability in the liquefaction opportunity depending on the local geology. This can be done approximately by evaluating the integral en in (4), i.e., $F(\omega)$, as a function of geology (via the site condition parameter s or thickness of sediments h) and local soil conditions. The effect on the microzonation maps would be an increase of opportunity at sites on sediments and a decrease at sites on basement rock. This will be illustrated in this paper.

The Los Angeles metropolitan area, for which results of microzonation are illustrated in this paper, was recently shaken by the Northridge earthquake (January 17, 1994; $M = 6.7$). Ground motion was recorded by more than 200 strong motion stations at a wide range of distances from the source. Analyses of the strong motion data suggest a reduction of peak acceleration at soft soil sites at distances up to about 30 km from the source for the horizontal component of motion, due to nonlinear soil response (Trifunac and Todorovska 1996, 1998a). The data on pipe breaks and observed soil distress are in favor of this hypothesis. Smooth contour maps of peak amplitudes of motion and response spectrum amplitudes indicate clear and strong effects of the deeper geologic structure, such as the amplification or reduction of amplitudes due to the constructive and destructive interference of waves reflected from the boundaries of the geologic basement and sharp vertical discontinuities along faults, and the slower attenuation rates in the Los Angeles Basin, due to “channeling” of wave energy (Todorovska and Trifunac 1997a,b).

Probability Distribution Function for N_{crit} and Cutoff Criteria

For specified σ_0 and ground shaking (en), (6) gives the critical value of \bar{N} for liquefaction to occur (if \bar{N} at the site is smaller than \bar{N}_{crit}). This value will be denoted by \bar{N}_{crit} . Eq. (6) can also be viewed as the borderline that separates the cases of liquefaction from those of no liquefaction. By measuring the distance from this borderline of the data points that violated the predictions by the models, Trifunac (1995) determined approximately the distribution of \bar{N}_{crit} . He approximated the distribution of the residuals ($\bar{N} - \bar{N}_{mod}$) by the normal probability distribution function, with mean μ_{res} and standard deviation σ_{res} . For the “en” model, $\mu_{res} = -1.95$ and $\sigma_{res} = 5.45$. The limited amount of data did not allow a rigorous statistical analysis and a search for the most representative distribution function.

Treating \bar{N}_{crit} as a random variable allows specifying the liquefaction criterion probabilistically. The probability that liquefaction will occur at a site, characterized by a corrected SPT value \bar{N} , is equal to the probability that the $\bar{N}_{crit} > \bar{N}$. For Gaussian \bar{N}_{crit}

$$\text{Prob}\{\bar{N}_{crit} > \bar{N}\} = \frac{1}{\sqrt{2\pi}\sigma} \int_{\bar{N}}^{\infty} \exp\left\{-\frac{1}{2}\left(\frac{x - \mu}{\sigma}\right)^2\right\} dx \quad (7)$$

The mean and standard deviations for \bar{N}_{crit} are

$$\mu = \bar{N}_{mod} + \mu_{res} \quad \text{and} \quad \sigma = \sigma_{res} \quad (8a,b)$$

where \bar{N}_{mod} = prediction by the model [given by (6) for the “en” model]; and μ_{res} and σ_{res} = mean and standard deviation of the distribution of the residuals, respectively. Fig. 3 shows a plot, versus earthquake magnitude, of the mean of N_{crit} for the “en” model, for $\sigma_0 = 50$ kPa and for hypocentral distances of 10, 40, and 100 km [the dependence on the representative distance (Trifunac and Lee 1990), is implicit in the evaluation of N_{crit}].

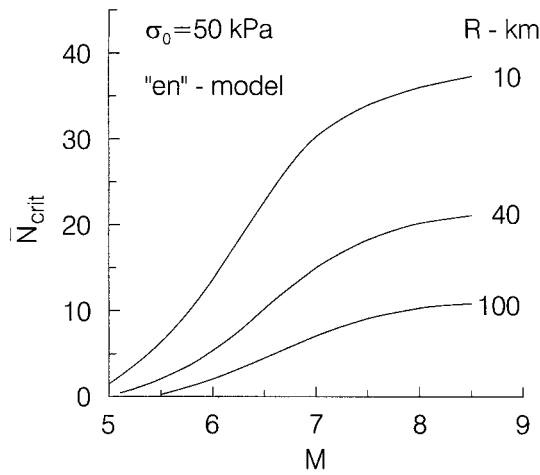


FIG. 3. Critical Corrected SPT Values \bar{N}_{crit} versus Earthquake Magnitude M as Predicted by "en" Model for Overburden Pressure $\sigma_0 = 50$ kPa, and at Distances $R = 10, 40,$ and 100 km from Source

In this paper, a normalized truncated Gaussian distribution was used as follows. The tails of the density function of \bar{N}_{crit} are cut off at $\bar{N}_{crit} = \mu \pm \sigma$, then the density function is adjusted so that it is zero at $\bar{N}_{crit} = \mu \pm \sigma$ and the area under the density function is equal to one (Todorovska 1996). Also, for sites with small \bar{N} , additional adjustments are made. If the earthquake size is so small and it is so far from the site that $\bar{N}_{crit} < 0$, it is assumed that it will not liquefy the site. If the earthquake is such that $N_{crit} < \sigma$, then the probability density function is further modified so that the left tail is cut off at $\bar{N} = 0$, and it is normalized so that the area under the density function is equal to one. In addition to this, other threshold criteria are applied for the earthquake magnitude and distance. It is assumed that the threshold magnitude for liquefaction to occur is $M = 4.75$. The distance cutoff criterion is described as follows.

Plots of earthquake magnitude versus distance for cases of observed liquefaction suggest that there may exist some maximum distance, magnitude dependent $R_{max}(M)$, beyond which earthquakes will not cause liquefaction (Kuribayashi and Tatsuoka 1975; Youd and Perkins 1978; Seed et al. 1984; Tinsley et al. 1985; Ambraseys 1988; Youd 1991). The database of documented cases of liquefaction is limited and incomplete, and the distances $R_{max}(M)$ will increase with time, as the observation period increases and the database becomes more complete. The distances for future liquefaction at very soft sites will likely surpass most of the currently defined $R_{max}(M)$. Therefore, the cutoff distance must be treated as a function of the in situ strength of the soil and all of the local factors (Yegian and Whitman 1978). The maximum distance in this paper is defined based on the premise that there is some threshold energy, dependent on \bar{N} and σ_0 , below which liquefaction will not occur at the site. This energy is expressed via a threshold value of en , $en_{threshold}$. The value of $en_{threshold}$ is related to the earthquake magnitude and distance and the site characteristics, via

$$en_{threshold} = \int_0^{\infty} \left(\frac{F(\omega, R_{max}, M, \text{site characteristics})}{\omega} \right)^2 d\omega \quad (9)$$

and to the site characteristics \bar{N} and σ_0 , via

$$en_{threshold} = \sigma_0^{3/2} \left(\frac{\bar{N} + \mu_{res}}{c} \right)^n \quad (10)$$

Eq. (9) follows from the definition of en , and gives the threshold en to be supplied by the earthquake. Eq. (10) follows from (6) and (7), and represents the minimum en required for the

TABLE 2. Cutoff Distances (km)

M (1)	$\log(en) = -2.8^a$ (2)	Seed et al. (1984) (3)	Tinsley et al. (1985) (4)	Ambraseys (1988) (5)
5.0	3.3	15.1	1.0	2.35
5.5	19.0	25.8	2.7	6.76
6.0	56.0	43.9	7.2	17.80
6.5	105.0	74.9	19.2	38.90
7.0	141.0	127.6	51.5	70.00
7.5	177.0	217.5	138.0	106.00
8.0	187.0	370.7	138.0	143.00
8.5	195.0	631.7	138.0	184.00

^aFor site on 1-km-thick sediments.

site to liquefy. Then, from (9) and (10), distances $R_{max}(M, \bar{N}, \sigma_0)$ can be computed once $en_{threshold}$ is specified. Based on the data tabulated by Berrill and Davis (1985), we adopted the value $en_{threshold} = 10^{-2.8} \text{ m}^2/\text{s}$ for the calculations in this paper. Table 2 shows $R_{max}(M)$ corresponding to $en_{threshold} = 10^{-2.8} \text{ m}^2/\text{s}$, for a site underlain by 1-km-thick alluvium. For comparison, $R_{max}(M)$ defined by Seed et al. (1984), Tinsley et al. (1985), and Ambraseys (1988) are also shown. Validation against the data for our choice of $en_{threshold}$, and implications for seismic hazard estimates of different $R_{max}(M)$ curves will be presented in a separate paper.

Hazard Model

The hazard is evaluated as follows. The locations of epicenters of possible earthquakes are discretized, as well as their magnitudes. Indices k are assigned to the magnitude values, and indices l to distances to possible ruptures. An earthquake of type (l, k) then refers to an event of magnitude M_k at distance R_l . The expected number of times that m_{Liq} liquefaction will occur at a site during exposure of t years is

$$m_{Liq}(\bar{N}, \sigma_0, t) = \sum_{l=1}^L \sum_{k=1}^K n_{lk}(t) q_{Liq,lk}(\bar{N}, \sigma_0) \quad (11)$$

In (11), $n_{lk}(t)$ = expected number of earthquakes of type (l, k) to occur during exposure of t years; and $q_{Liq,lk}$ = conditional probability that liquefaction will occur given that an earthquake of type (l, k) has occurred. The expected number of earthquakes $n_{lk}(t)$ is evaluated from the expected number of earthquakes for the source zone the l th location belongs to, based on adopted rationale for the spatial distribution of the possible earthquakes within the zone (Todorovska and Lee 1995). The conditional probability $q_{Liq,lk}$ can be evaluated from (7). The average return period of liquefaction occurrence can be evaluated by dividing the exposure t by the average number of occurrences $m_{Liq}(\bar{N}, \sigma_0, t)$. The probability that liquefaction will occur during exposure t is

$$p(\bar{N}, \sigma_0, t) = 1 - e^{-m_{Liq}(\bar{N}, \sigma_0, t)} \quad (12)$$

Eqs. (11) and (12) can be easily generalized to also include sources with a time-dependent hazard rate for which the earthquake occurrence can be classified as a non-homogeneous Poissonian process (Todorovska 1994a,b).

RESULTS AND DISCUSSION

The Los Angeles metropolitan area is chosen to illustrate the proposed mapping methodology. The area with the major fault lines and hills and mountains [shown by gray areas, after Yerkes et al. (1965)] is shown in Fig. 4, and it is also shown in Fig. 1 by a hatched rectangle. The local geologic conditions, characterized by thickness of sediments h are shown in Fig. 5 at a grid of points equally spaced at 5-min intervals (Yerkes

Los Angeles Basin

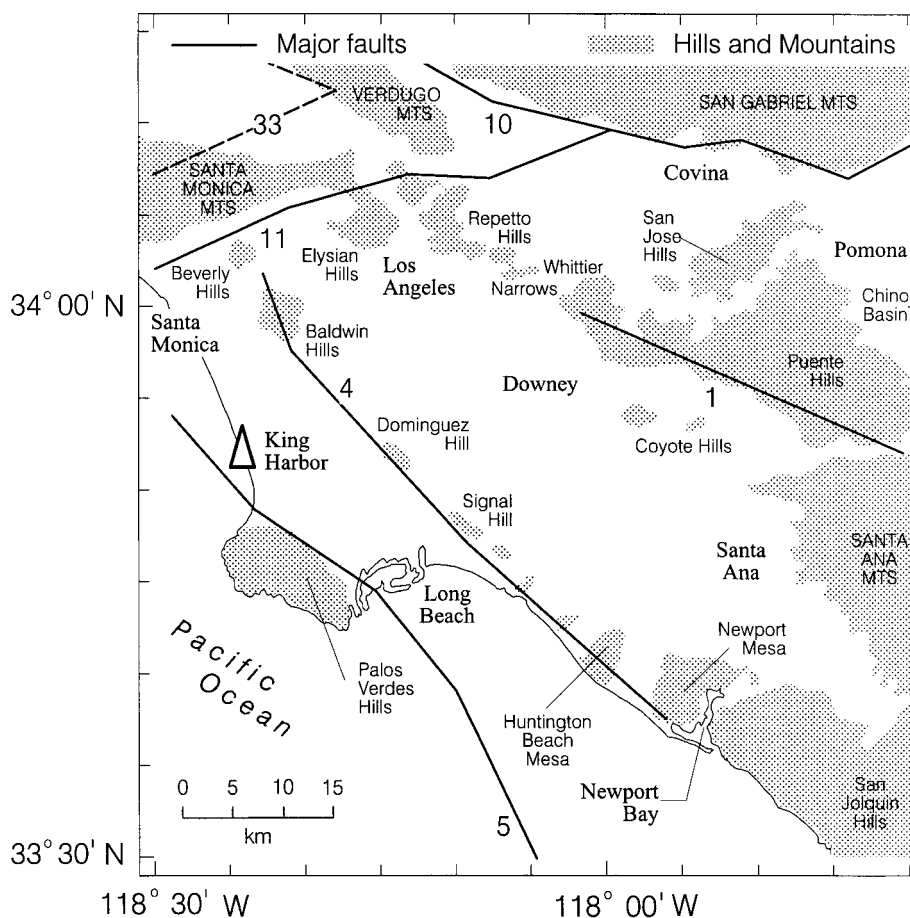


FIG. 4. Los Angeles Metropolitan Area, Considered for Microzoning in this Paper, with Some of Major Cities, Fault Lines of Seismicity Model (Table 1) and Outlines of Hills and Mountains [Shown by Gray Areas as per Yerkes et al. (1965)]

et al. 1965; Lee and Trifunac 1987). The number at each node of the grid is the depth to basement rock in kilometers. For the purpose of this paper, the results were evaluated at these grid points and were then interpolated at a denser grid to define the contours. The computer code NEQRISK (Lee and Trifunac 1985) was used for the calculations.

For use in engineering applications, e.g., microzoning of a metropolitan area, it would be necessary to model the geometry of the seismic sources in more detail [using the full 3D capabilities of NEQRISK (Todorovska and Lee 1995)], possibly with the use of time-dependent earthquake occurrence models (Todorovska 1994a,b), provide more detailed input on the local soil and geologic conditions, and evaluate the liquefaction opportunity at a denser set of grid points. Such a detailed analysis is beyond the scope of this paper. However, the overall features and trends of the microzoning maps presented here are not expected to change much when such detailed information is considered.

Fig. 6 shows the distribution of the average return period of liquefaction for $\bar{N} = 10$ and $\sigma_0 = 40$ kPa, assumed everywhere in the area, and for thickness of sediments h assumed to be zero (i.e., all sites are assumed to be at basement rock). A longer return period indicates a smaller opportunity, and vice versa. It is seen that the return period varies between 80 years (toward the northeast corner of the region) and 170 years (along the Pacific coast). For this case, the results depend significantly on the distance from the faults and their activity. Although there are some variations depending on the distance from the local faults, the contributions from the San Andreas Fault dominate the hazard. Fig. 7 shows the average return

period of liquefaction for the same area if the thickness of sediments is considered (Fig. 5). It is seen that the return period is in the range from 30 to 80 years in the San Gabriel Valley and from 20 to 30 years in the Los Angeles Basin (between the Whittier-Elsinore and the Newport-Inglewood Faults). Differences between the results shown in Figs. 6 and 7 are caused by: (1) larger amplitudes of strong motion velocities (Trifunac 1976b); and (2) a longer duration of strong motion (Novikova and Trifunac 1993, 1995) on deeper sediments, both contributing to larger wave energy in the soil. The sediments are deeper away from the two faults and reach a maximum depth of about 9 km (Fig. 5). Similar effects of increased hazard in the Los Angeles Basin have been observed in microzoning maps for peak spectral amplitudes and peak surface strain (Lee and Trifunac 1987; Trifunac 1988, 1990b; Todorovska and Trifunac 1996). Increased amplitudes are also observed in contour maps of peak acceleration, velocity, and displacement, and in pseudo spectral velocity (PSV) amplitudes during the 1994 Northridge earthquake, based on information from recorded strong ground motion (Todorovska and Trifunac 1997a,b). Fig. 8 shows the return period for $\bar{N} = 20$ and $\sigma_0 = 40$ kPa. It is seen that as σ_0 in the soil increases (relative to Fig. 7), the amplification effects by deeper sediments become progressively less important, and the hazard is progressively more governed by the San Andreas Fault.

Another way of presenting a spatial distribution of hazard is to map \bar{N} for which liquefaction will occur, during the exposure period, with equal probability everywhere in the region (σ_0 is again a parameter with an assigned value). Fig. 9 shows such a map for a 10% probability to liquefy during 50 years'

Los Angeles Basin: depth of sediments - km

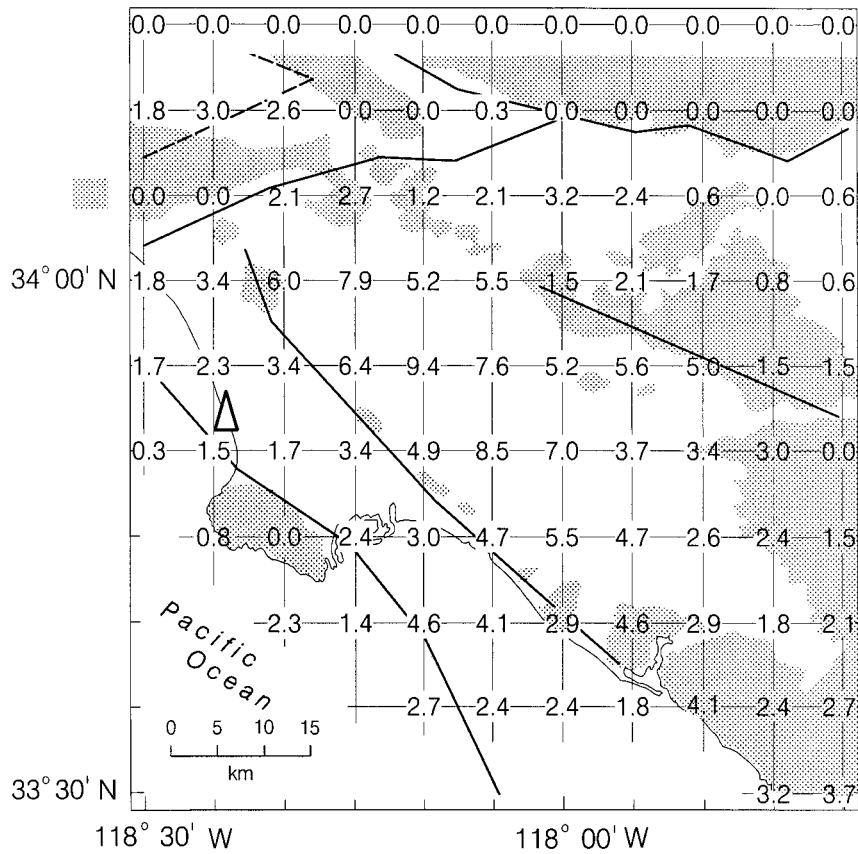


FIG. 5. Thickness of Sedimentary Deposits in Los Angeles Metropolitan Area at Grid of Points with 5' Interval [Major Faults Are Shown by Heavy Lines, and Hills and Mountains by Gray Areas, after Yerkes et al. (1965)]

Expected Return Period of Liquefaction - yrs
 $\bar{N} = 10, \sigma_0 = 40 \text{ kPa}$ depth of sediments $h=0$

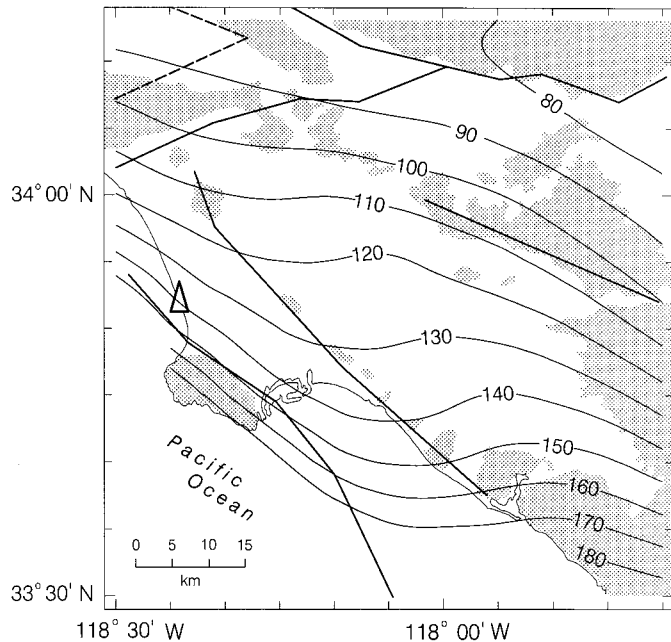


FIG. 6. Map of Average Return Period of Liquefaction (as Predicted by "en" Model) for $\bar{N} = 10, \sigma_0 = 40 \text{ kPa}$, and Thickness of Sediments $h = 0$ Everywhere in Region (Major Faults Are Shown by Heavy Lines, and Hills and Mountains by Gray Areas)

Expected Return Period of Liquefaction - yrs
 $\bar{N} = 10, \sigma_0 = 40 \text{ kPa}$ depth of sediments $h \neq 0$

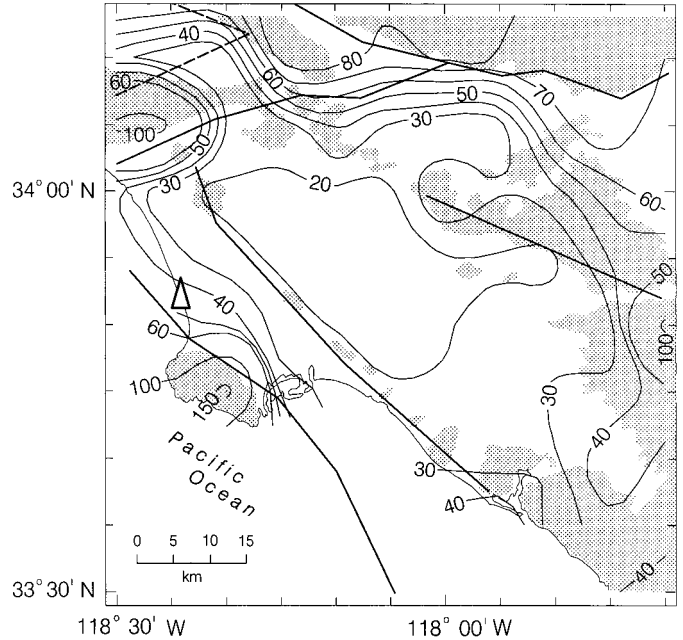


FIG. 7. Map of Average Return Period of Liquefaction (as Predicted by "en" Model) for $\bar{N} = 10, \sigma_0 = 40 \text{ kPa}$, and Thickness of Sediments h , as in Fig. 5 (Major Faults Are Shown by Heavy Lines, and Hills and Mountains by Gray Areas)

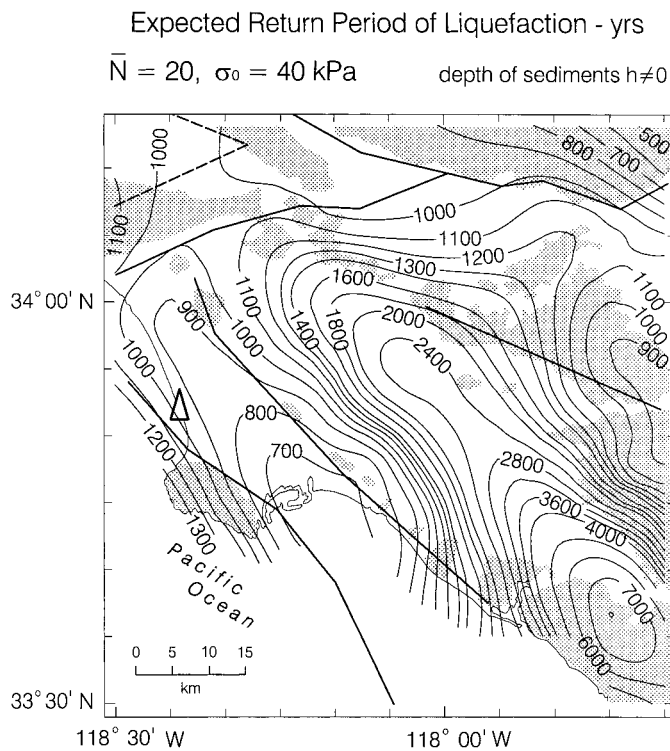


FIG. 8. Map of Average Return Period of Liquefaction (as Predicted by "en" Model) for $\bar{N} = 20, \sigma_0 = 40 \text{ kPa}$, and Thickness of Sediments h , as in Fig. 5 (Major Faults Are Shown by Heavy Lines, and Hills and Mountains by Gray Areas)

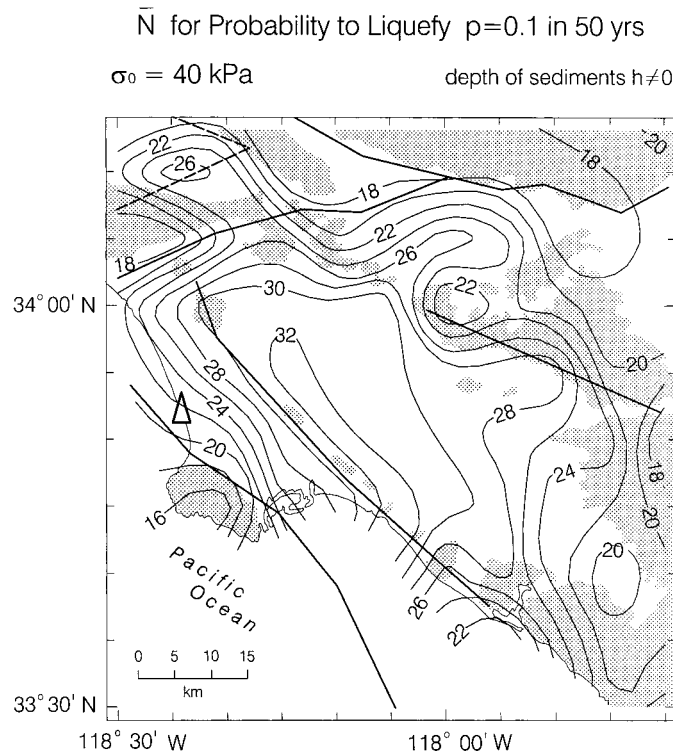


FIG. 9. Map of \bar{N} (as Predicted by "en" Model) for Probability of Occurrence $p = 0.1, \sigma_0 = 40 \text{ kPa}$, and Thickness of Sediments h , as in Fig. 5

exposure to seismic activity, and for $\sigma_0 = 40 \text{ kPa}$. Dependence on the thickness of the sediments is included. In Fig. 9, \bar{N} varies between 16 (in the Santa Monica Mountains, San Gabriel Mountains, and Palos Verdes Peninsula) and 32 (north-east and along the Newport-Inglewood Fault Zone (No. 4 in

Fig. 4), north of Dominguez Hill, and northwest of Huntington Beach Mesa).

Plots of the expected number of liquefaction occurrences $m_{\text{Liq}}(\bar{N}, \sigma_0, t)$ of the return period $T_{\text{Liq}}(\bar{N}, \sigma_0)$ and the probability of liquefaction $p(\bar{N}, \sigma_0, t)$ provide useful information in analyses of liquefaction hazards at a site. Fig. 10 illustrates such plots versus a corrected SPT value \bar{N} for a site at King Harbor (shown by a triangle in Figs. 4–9), for exposure $t = 50$ years, and for $\sigma_0 = 20, 40, 80$, and 160 kPa . This site is in an area characterized by Tinsley et al. (1985) as being highly susceptible to liquefaction, and liquefaction was observed there during the 1994 Northridge earthquake. Plots such as those in Fig. 10 would show, e.g., at locations where site improvement is planned, how the hazard would change with the degree of strengthening.

An efficient way to store the information on the spatial distribution of liquefaction hazard is via maps (Figs. 7–9), for a range of \bar{N} and σ_0 values, and of the probability of occurrence p . From a series of such maps, by reading the value of T_{Liq} at a particular site, one can construct T_{Liq} as a function of \bar{N} for that site. Similarly, from a series of equal probability maps, one can construct p as a function of \bar{N} (Todorovska 1998).

Smaller \bar{N} and σ_0 indicates higher liquefaction susceptibility. For values of σ_0 larger than 40 kPa and values of \bar{N} larger than 10, maps such as those in Figs. 7 and 8 will show longer return periods. For values of σ_0 larger than 20 kPa and/or $p < 0.1$, maps such as that shown in Fig. 8 will show larger values of \bar{N} .

The results in Fig. 7 are in qualitative agreement with those of Tinsley et al. (1985), whose zoning was based on the maximum distance-magnitude criterion, and can be compared with our results for susceptible sites (small \bar{N}). Based on this simple empirical criterion, the area considered in this paper is within the 30 years return period zone.

The criterion for liquefaction used in this paper is defined by a probabilistic distribution function rather than by "yes" or "no," and is therefore sensitive to different degrees of liquefaction susceptibility, and also to the site geology (which influences the amplitudes and duration of ground motion). Therefore, it leads to more detailed and more general zoning maps than those based on the maximum distance-magnitude criterion.

SUMMARY AND CONCLUSIONS

A probabilistic method for liquefaction opportunity mapping during specified exposure is presented. The condition leading to liquefaction is governed by a physical model of seismic wave energy, calculated via broadband Fourier amplitude spectra of ground acceleration (Trifunac 1993, 1994). The minimum magnitude that can initiate liquefaction is assumed to be $M = 4.75$. For the examples shown in this paper, a maximum limit for the distance for liquefaction to occur is defined by an empirical estimate of a threshold value of the energy factor $en = \int_{0.0628}^{628} (F(\omega)/\omega)^2 d\omega$ equal to $10^{-2.8} \text{ m}^2/\text{s}$. Examples of microzoning are presented for the Los Angeles metropolitan area, for a seismicity model described in this paper. This model assumes that the earthquakes occur in cycles with exponentially distributed interoccurrence intervals. The earthquake rates predicted by the seismicity model are consistent with the observed rate since the year 1850. The presented results illustrate the variability governed by the geologic site conditions, via thickness of sediments.

The purpose of this paper has been to explore the possibilities of using energy-based probabilistic assessment for liquefaction occurrence for microzoning mapping, and to illustrate the methodology. The Los Angeles metropolitan area has been chosen for the illustrations. The maps of the average return period of liquefaction show variations between 30 and

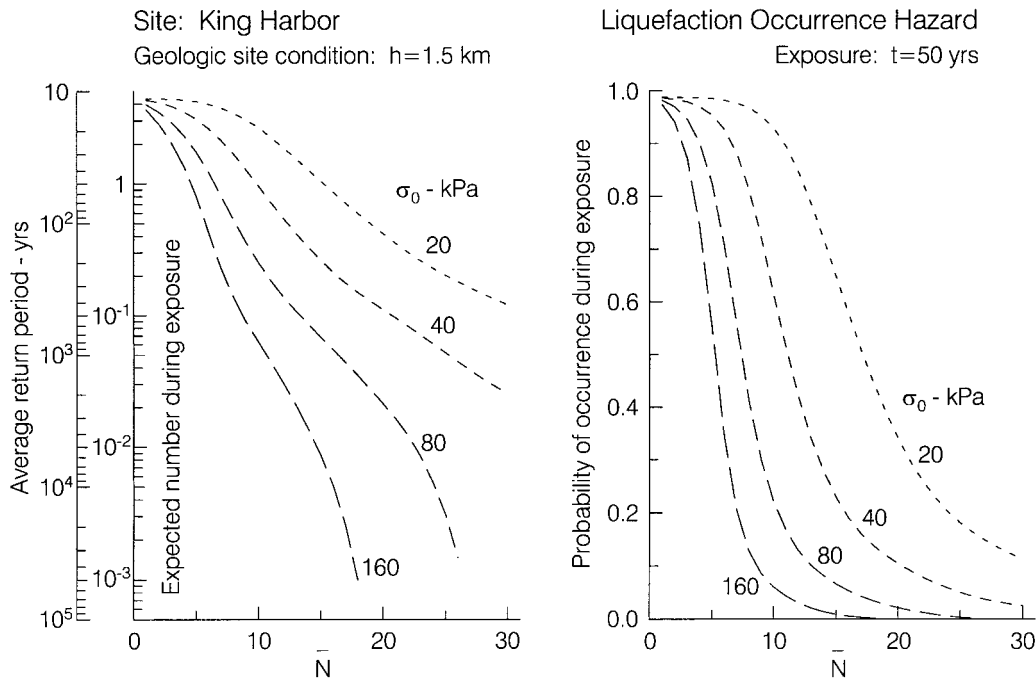


FIG. 10. Results for Site at King Harbor (Fig. 4), for 50 Years' Exposure: Return Period of Liquefaction, Expected Number of Occurrences and Probability of Occurrence, All versus Corrected SPT Value \bar{N} . Different Types of Lines Correspond to Overburden Pressure $\sigma_0 = 20, 40, 80,$ and 160 kPa

80 years, for $\bar{N} = 10$ and $\sigma_0 = 40$ kPa. The equal probability map shows that for $\sigma_0 = 40$ kPa and 50 years' exposure, and for 0.1 probability of occurrence, \bar{N} varies between 16 and 32 counts per foot. The maps show that the San Andreas Fault has a prominent contribution to the hazard. The hazard is also larger in the San Gabriel Valley and Los Angeles Basin, due to the amplification of ground motion amplitudes and a longer duration of shaking in sediments.

Detailed results (plots of return period of liquefaction, expected number of occurrences in 50 years' exposure, and probability of occurrence, all versus the corrected SPT value and for several values of the overburden pressure) are illustrated for a site at King Harbor, where liquefaction occurred during the 1994 Northridge earthquake. Such curves can be constructed from a series of microzonation maps for different values of the parameters (Todorovska 1998).

In actual applications, maps will be used that consider greater detail in the geometry of the seismic sources, and more detailed specification of the site geology. This will lead to more detail in the computed contours, but the overall regional amplitudes will not differ qualitatively from the maps presented in this paper. The input on the earthquake occurrence rates can also be updated as new information becomes available. The method can be improved further by studying in more detail the threshold conditions for the energy-based liquefaction occurrence criterion.

The simple site characterization makes this method very attractive for hazard mapping purposes. The type of maps shown in this paper shows the liquefaction opportunity for a range of site properties. For liquefaction to occur, there should be a liquefiable layer at the site. Liquefaction potential can be mapped by overlaying opportunity with susceptibility maps (based on geology, geotechnical data, and eventually water table maps). For a specific project, after \bar{N} and σ_0 are estimated for the site, the probability for liquefaction occurrence (or the average return period of liquefaction) can be read directly or estimated by interpolation from the appropriate liquefaction opportunity map(s). A series of opportunity maps can be used to construct the return period of liquefaction as a function of \bar{N} , or the probability of liquefaction as a function of \bar{N} [both

for selected values of σ_0 (Todorovska 1998)]. Such curves can be used in cost benefit analyses and in decision-making processes related to ground improvement projects.

APPENDIX. REFERENCES

- Algermissen, S. T., and Perkins, D. M. (1976). "A probabilistic estimate of maximum acceleration in rock in the contiguous United States." *Open File Rep. 76-416*, U.S. Dept. of the Interior, Geological Survey.
- Ambraseys, N. N. (1988). "Engineering seismology." *Earthquake Engrg. and Struct. Dynamics*, 7, 70–105.
- Atkinson, G. M., Finn, W. D. L., and Charlwood, R. G. (1984). "Simple computation of liquefaction probability for seismic hazard applications." *Earthquake Spectra*, 1(1), 107–123.
- Benioff, H. (1934). "A physical evaluation of seismic destructiveness." *Bull. Seismological Soc. of Am.*, 24, 389–403.
- Berrill, J. B., and Davis, R. O. (1985). "Energy dissipation and seismic liquefaction of sands: Revised model." *Soils and Found.*, Tokyo, 25(2), 106–118.
- Blazquez, R. M., Krizek, R. J., and Bazant, Z. P. (1980). "Site factors controlling liquefaction." *J. Geotech. Engrg. Div.*, ASCE, 106(7), 785–801.
- Davis, R. O., and Berrill, J. B. (1982). "Energy dissipation and seismic liquefaction in sands." *Earthquake Engrg. and Struct. Dynamics*, 10, 51–68.
- Fischhoff, B., Lichtenstein, S., Slovic, P., Derby, S. L., and Keeney, R. (1981). *Acceptable risk*. Cambridge University Press, Cambridge, Mass.
- Holzer, T. L., Youd, T. L., and Hanks, T. C. (1989). "Dynamics of liquefaction during the 1987 Superstition Hills, California, Earthquake." *Sci.*, 244, 56–59.
- Kavazanjian, E., Jr., Roth, R. A., and Echezuria, H. (1985). "Liquefaction potential mapping for San Francisco." *J. Geotech. Engrg.*, ASCE, 111(1), 54–76.
- Kayen, R. E., and Mitchell, J. K. (1997). "Assessment of liquefaction potential during earthquakes, by Arias intensity." *J. Geotech. and Geoenviron. Engrg.*, ASCE, 123(12), 1162–1174.
- Kramer, S. L. (1996). *Geotechnical earthquake engineering*. Prentice-Hall, Englewood Cliffs, N.J.
- Kuribayashi, E., and Tatsuoka, F. (1975). "Brief review of liquefaction during earthquakes in Japan." *Soils and Found.*, 15, 81–92.
- Lee, V. W. (1993). "Scaling PSV from earthquake magnitude, local soil and geological depth of sediments." *J. Geotech. Engrg.*, ASCE, 119(1), 108–126.
- Lee, V. W., Amini, A., and Trifunac, M. D. (1982). "Noise in earthquake accelerograms." *J. Engrg. Mech. Div.*, ASCE, 108(6), 1121–1129.

- Lee, V. W., and Trifunac, M. D. (1985). "Uniform risk spectra of strong earthquake ground motion: NEQRISK." *Rep. CE 85-05*, Dept. of Civ. Engrg., University of Southern California, Los Angeles.
- Lee, V. W., and Trifunac, M. D. (1987). "Microzonation of a metropolitan area." *Rep. CE 87-02*, Dept. of Civ. Engrg., University of Southern California, Los Angeles.
- Lee, V. W., and Trifunac, M. D. (1995a). "Frequency dependent attenuation function and Fourier amplitude spectra of strong earthquake ground motion in California." *Rep. CE 95-03*, Dept. of Civ. Engrg., University of Southern California, Los Angeles.
- Lee, V. W., and Trifunac, M. D. (1995b). "Pseudo relative velocity spectra of strong earthquake ground motion in California." *Rep. CE 95-04*, Dept. of Civ. Engrg., University of Southern California, Los Angeles.
- Lee, V. W., Trifunac, M. D., Todorovska, M. I., and Novikova, E. I. (1995). "Empirical equations describing attenuation of the peaks of strong ground motion, in terms of magnitude, distance, path effects and site conditions." *Rep. CE 95-02*, Dept. of Civ. Engrg., University of Southern California, Los Angeles.
- Novikova, E. I., and Trifunac, M. D. (1993). "Duration of strong earthquake ground motion: Physical basis and empirical equations." *Rep. CE 93-02*, Dept. of Civ. Engrg., University of Southern California, Los Angeles.
- Novikova, E. I., and Trifunac, M. D. (1995). "Frequency dependent duration of strong earthquake ground motion: Updated empirical equations." *Rep. CE 95-01*, Dept. of Civ. Engrg., University of Southern California, Los Angeles.
- Papaulis, A. (1962). *The Fourier integral and its applications*. McGraw-Hill, New York.
- Richter, C. F. (1958). *Elementary seismology*. Freeman, San Francisco.
- Robertson, P. K., and Capanella, R. G. (1985). "Liquefaction potential of sands using CPT." *J. Geotech. Engrg.*, ASCE, 111(3), 384–403.
- Robertson, P. K., Woeller, D. J., and Finn, W. D. L. (1992). "Seismic cone penetration tests for evaluating liquefaction potential under cycling loading." *Can. Geotech. J.*, Ottawa, 29(4), 686–695.
- Seed, H. B., Tokimatsu, K., Harder, L., and Chung, R. (1984). "The influence of SPT procedures on soil liquefaction resistance evaluations." *Rep. No. 84-15*, Earthquake Engrg. Res. Ctr., University of California, Berkeley, Calif.
- Shibata, S., and Teparaksa, W. (1988). "Evaluation of liquefaction potentials of soils using cone penetration tests." *Soils and Found.*, 28(2), 49–60.
- Tinsley, J. C., Youd, T. L., Perkins, D. M., and Chen, A. T. F. (1985). "Evaluating liquefaction potential." *U.S. Geological Survey Prof. Paper 1360*, 263–315.
- Todorovska, M. I. (1994a). "Comparison of response spectrum amplitudes from earthquakes with lognormally and exponentially distributed return period." *Soil Dyn. and Earthquake Engrg.*, 13(2), 97–116.
- Todorovska, M. I. (1994b). "Order statistics of functionals of strong ground motion for a class of renewal processes." *Soil Dyn. and Earthquake Engrg.*, 13(6), 399–405.
- Todorovska, M. I. (1995a). "Effects of earthquake source parameters on uniform probability response spectra." *Proc., 10th Eur. Conf. Earthquake Engrg.*, Vol. 4, Balkema, Rotterdam, The Netherlands, 2579–2584.
- Todorovska, M. I. (1995b). "Uniform probability response spectra for selecting site specific design motions." *Proc., 3rd Int. Conf. on Recent Adv. in Geotech. Earthquake Engrg. and Soil Dyn.*, Vol. II, 613–618.
- Todorovska, M. I. (1996). "Liquefaction hazard assessment via seismic wave energy and SPT values." *Eur. Earthquake Engrg.*, 10(2), 24–37.
- Todorovska, M. I. (1998). "Quick reference liquefaction opportunity maps for a metropolitan area." *Geotechnical earthquake engineering and soil dynamics III, Geotech. Spec. Publ. No. 75*, Vol. 1, ASCE, Reston, Va., 116–127.
- Todorovska, M. I., Gupta, I. D., Gupta, V. K., Lee, V. W., and Trifunac, M. D. (1995). "Selected topics in probabilistic seismic hazard assessment." *Rep. CE 95-08*, Dept. of Civ. Engrg., University of Southern California, Los Angeles.
- Todorovska, M. I., and Lee, V. W. (1995). "A note on sensitivity of uniform probability spectra on modeling the fault geometry in areas with a shallow seismogenic zone." *Eur. Earthquake Engrg.*, 9(2), 14–22.
- Todorovska, M. I., and Trifunac, M. D. (1996). "Hazard mapping of normalized peak strain in soil during earthquakes: Microzonation of a metropolitan area." *Soil Dyn. and Earthquake Engrg.*, 15(5), 321–329.
- Todorovska, M. I., and Trifunac, M. D. (1997a). "Distribution of pseudo spectral velocity during the Northridge, California, earthquake of 17 January, 1994." *Soil Dyn. and Earthquake Engrg.*, 16(3), 173–192.
- Todorovska, M. I., and Trifunac, M. D. (1997b). "Amplitudes, polarity and time of peaks of strong ground motion during the 1994 Northridge, California, earthquake." *Soil Dyn. and Earthquake Engrg.*, 16(4), 235–258.
- Trifunac, M. D. (1972). "Tectonic stress and the source mechanism of the Imperial Valley, California, Earthquake of 1940." *Bull. Seismological Soc. of Am.*, 62(5), 1283–1302.
- Trifunac, M. D. (1976a). "Preliminary empirical model for scaling Fourier amplitude spectra of strong ground acceleration in terms of earthquake magnitude, source to station distance, and recording site conditions." *Bull. Seismological Soc. of Am.*, 66(9), 1343–1373.
- Trifunac, M. D. (1976b). "Preliminary analysis of the peaks of strong earthquake ground motion—Dependence of peaks on earthquake magnitude, epicentral distance and the recording site conditions." *Bull. Seismological Soc. of Am.*, 66, 187–219.
- Trifunac, M. D. (1988). "Seismic microzonation mapping via uniform risk spectra." *Proc., 9th World Conf. on Earthquake Engrg.*, Vol. VIII, 75–80, Tokyo-Kyoto, Maruzen Co. Ltd., Tokyo, Japan.
- Trifunac, M. D. (1990a). "How to model amplification of strong earthquake motion by local geologic and soil site conditions." *Earthquake Engrg. and Struct. Dynamics*, 19(6), 833–846.
- Trifunac, M. D. (1990b). "A microzonation method based on uniform risk spectra." *Soil Dyn. and Earthquake Engrg.*, 9(1), 34–43.
- Trifunac, M. D. (1993). "Long period Fourier amplitude spectra of strong motion acceleration." *Soil Dyn. and Earthquake Engrg.*, 12(6), 363–382.
- Trifunac, M. D. (1994). "Q and high frequency strong motion spectra." *Soil Dyn. and Earthquake Engrg.*, 13(3), 149–161.
- Trifunac, M. D. (1995). "Empirical criteria for liquefaction in sands via standard penetration tests and seismic wave energy." *Soil Dyn. and Earthquake Engrg.*, 14(6), 419–426.
- Trifunac, M. D. (1999). "Discussion of 'Assessment of liquefaction potential during earthquakes,' by R. E. Kayen and J. K. Mitchell." *J. Geotech. and Geoenviron. Engrg.*, ASCE, 125(7), 627.
- Trifunac, M. D., and Brady, A. G. (1975). "A study on the duration of strong earthquake ground motion." *Bull. Seismological Soc. of Am.*, 65(3), 581–626.
- Trifunac, M. D., and Lee, V. W. (1966). "Peak surface strains during strong earthquake motion." *Soil Dyn. and Earthquake Engrg.*, 15(5), 311–319.
- Trifunac, M. D., and Lee, V. W. (1990). "Frequency dependent attenuation of strong earthquake ground motion." *Soil Dyn. and Earthquake Engrg.*, 9(1), 3–15.
- Trifunac, M. D., and Novikova, E. I. (1995). "State of the art review of strong motion duration." *Proc., 10th Eur. Conf. Earthquake Engrg.*, Vol. 1, Balkema, Rotterdam, The Netherlands, 131–140.
- Trifunac, M. D., and Todorovska, M. I. (1996). "Nonlinear soil response—1994 Northridge, California, earthquake." *J. Geotech. Engrg.*, ASCE, 122(9), 725–735.
- Trifunac, M. D., and Todorovska, M. I. (1998a). "Nonlinear soil response as a natural passive isolation mechanism—1994 Northridge, California, earthquake." *Soil Dyn. and Earthquake Engrg.*, 17(1), 41–51.
- Trifunac, M. D., and Todorovska, M. I. (1998b). "Amplification of strong ground motion and damage patterns during the 1994 Northridge, California, earthquake." *Proc., Spec. Conf. on Geotech. Engrg. and Soil Dyn., Geotech. Spec. Publ. No. 75*, Vol. I, ASCE, Reston, Va., 714–725.
- Trifunac, M. D., and Todorovska, M. I. (1998c). "Damage distribution during the 1994 Northridge, California, earthquakes relative to generalized categories of surficial geology." *Soil Dyn. and Earthquake Engrg.*, 17(4), 239–253.
- Working group on California earthquake probabilities. (1995). "Seismic hazards in southern California: Probable earthquakes, 1994 to 2024." *Bull. Seismological Soc. of Am.*, 85(2), 379–439.
- Yegian, M. K., and Whitman, R. V. (1978). "Risk analysis for ground failure by liquefaction." *J. Geotech. Engrg. Div.*, ASCE, 104(7), 921–938.
- Yerkes, R. F., McCulloh, T. H., Schoellhamer, J. E., and Vedder, J. G. (1965). "Geology of the Los Angeles Basin, California—An introduction." *U.S. Geological Survey Prof. Paper 420-A*.
- Youd, L. T. (1991). "Mapping of earthquake induced liquefaction for seismic zonation." *Proc., 4th Int. Conf. on Seismic Zonation*, Vol. I, 111–146.
- Youd, L. T., and Holzer, T. L. (1994). "Piezometer performance at wild-life liquefaction site, California." *J. Geotech. Engrg.*, ASCE, 120(6), 975–995.
- Youd, L. T., and Perkins, D. M. (1978). "Mapping liquefaction induced ground failure potential." *J. Geotech. Engrg. Div.*, ASCE, 104(4), 433–446.
- Youd, L. T., and Perkins, D. M. (1987). "Mapping of liquefaction severity index." *J. Geotech. Engrg.*, ASCE, 113(11), 1374–1392.